Real-Time Molecular Monitoring of Chemical Environment in Obligate

Anaerobes during Oxygen Adaptive Response

Hoi-Ying N. Holman[1,2]*, Eleanor Wozei[1,4], Zhang Lin[1,5], Luis R. Comolli[1], David. A. Ball[1],

Sharon Borglin[1,2], Matthew W. Fields[2,3], Terry C. Hazen[1,2], Kenneth H. Downing[1]

[1]Lawrence Berkeley National Laboratory, One Cyclotron Rd., Berkeley, CA, 94720, USA.

[2]Virtual Institute for Microbial Stress and Survival, http://vimss.lbl.gov.

[3]Montana State University, Bozeman, MT 59717, USA

[4]Current address: Makerere University, Kampala, Uganda

[5]Current address: Fujian Institute of Research on the Structure of Matter, Chinese Academy of

Sciences, Fujian, 350002, People's Republic of China

* Communicating Author

Hoi-Ying N. Holman, Ph.D.
MS. 70A-3317L
Lawrence Berkeley National Laboratory
One Cyclotron Road,
Berkeley, CA 94720
Phone: (510) 486-5943
Fax: (510) 486-7152
e-mail: hyholman@lbl.gov

Dual classification: Physical Sciences (chemistry) & Biological Sciences (microbiology)

Abstract length: 140 words or 967 characters (including space).

Manuscript length: 21 text pages (including space, materials/methods, and figure legends).

Figures: 6 figures.

Abstract

Determining the transient chemical properties of the intracellular environment can elucidate the paths through which a biological system adapts to changes in its environment, for example, the mechanisms which enable some obligate anaerobic bacteria to survive a sudden exposure to oxygen. Here we used high-resolution Fourier Transform Infrared (FTIR) spectromicroscopy to continuously follow cellular chemistry within living obligate anaerobes by monitoring hydrogen bonding in their cellular water. We observed a sequence of well orchestrated molecular events that correspond to changes in cellular processes in those cells that survive, but only accumulation of radicals in those that do not. We thereby can interpret the adaptive response in terms of transient intracellular chemistry and link it to oxygen stress and survival. This ability to monitor chemical changes at the molecular level can yield important insights into a wide range of adaptive responses.

\body

Significant progress has been made at the biochemical and genetic levels in our understanding of how some environmentally and medically important obligate anaerobes can survive temporarily a sudden exposure to oxygen molecules (1-6). However, our understanding at a cellular molecular level of the actual capacity and mechanisms of how these anaerobes survive remains incomplete (7). The cellular chemical environment fundamentally comprises the nexus between external stimuli and internal biochemical regulatory mechanisms - and affects many properties of cellular adaptive response as well. Determining this transient chemical environment *in vivo* is critical for achieving a more coherent understanding of how some obligate anaerobes adapt to the extreme fluctuations in oxygenation. Such knowledge is seldom complete because it is difficult to make *in-vivo* molecular measurements without disturbing cells. In almost all previous studies, cellular chemistry of oxygen-stress adaptive response has been determined by measuring intermediate reaction products in cell extracts taken at selected times (8-10); notably, ongoing changes within a live cell are seldom measured directly. The instability of many of the intermediates greatly complicates measurements of cell extracts and their analyses.

Here, we present results of our using the non-invasive synchrotron radiation-based Fourier Transform Infrared (FTIR) spectromicroscopy approach (11) to determine the cellular chemical environment by continuously monitoring the dynamics of hydrogen bonding in cellular water *in vivo*. More than 70% of the cellular constituents are highly polar water molecules, and their hydrogen bonding is a useful reflection of the cellular chemical environment because it responds "instantaneously" to ions and other species in their surroundings (12, 13). The infrared spectrum of OH stretch vibrations has been widely used to characterize the dynamics of hydrogen-bonding structures in pure water (13-23). These infrared spectroscopy studies have revealed distinct shifts

in vibration frequencies and changes in spectral shapes and intensities induced by the presence of ions and small molecules (e.g., radicals, small organic acids, and hydrogen gas) in water; similar small molecules are expected to be in cellular water during functional metabolism of oxygen-stress adaptive response.

In this study, we investigated the dynamics of cellular chemical environment in a model oxygen-stress adaptive response system, namely that of the strictly anaerobic sulfate-reducing bacterium *Desulfovibrio vulgaris* Hildenborough during transient exposure to air. Sulfate-reducing bacteria are of particular interest because of their importance in cycling and transformation of essential nutrients and minerals (24, 25) and of their links to different pathogenesis (26, 27) in environments where extreme fluctuations in oxygen concentrations occur. Among sulfate-reducing bacteria, genome sequencing has shown that *D. vulgaris* has developed well-defined protective enzymatic oxygen-defense systems (5, 24). The bacteria can even survive very high levels of oxygen in their natural environment (28, 29), but the mechanism remains elusive. We demonstrate here that molecular information provided by real-time, *in-vivo* FTIR measurements of the transient cellular chemical environment is critical for advancing a fundamental understanding of how these obligate anaerobes adapt to extreme changes during air exposure, by providing the first direct observations of molecular events measured in the same cells over time.

Results and Discussion

Identification of *D. vulgaris* cells that can survive temporarily in atmospheric oxygen. We first conducted microscopic and spectroscopic analyses to establish at a whole cell level the molecular identity of *D. vulgaris* cells that can survive transient exposure to atmospheric oxygen. This identity enabled us to select the appropriate cells for the real-time FTIR measurements of

the oxygen-stress survival response. Fluorescence microscopy images of two nucleic acid stains show that most stationary-phase (but not exponential-phase) *D. vulgaris* can survive short-term oxygen exposure. Subsequent electron microscopy images reveal that stationary-phase (but not exponential-phase) *D. vulgaris* accumulates polyglucose (Fig. 1A) and stores elemental sulfur particles (Fig. 1B). Their FTIR spectrum shows distinctly the non-glycosidic polyglucose vibration (υC–OH) band between 1055 and 1045 cm^{-1}, and the glycosidic linkage vibration (υC–O–C) at ~1175 cm^{-1} (30). These cells can survive air exposure for hours and resume growth when returned to anaerobic conditions (Fig. 1C), despite significant changes in cellular structures and contents (Figs. 1D and 1E).

FTIR measurement and analysis considerations. Mid-infrared photons emitted from the synchrotron at the Advanced Light Source in the Lawrence Berkeley National Laboratory (CA, USA) were focused through a 15-µm aperture onto a monolayer of stationary-phase *D. vulgaris* cells maintained inside an oxygen-free humidified microscope stage chamber (Fig. 2A). In Figure 2B is an FTIR spectrum typical of small groups of stationary-phase *D. vulgaris* cells, showing well-resolved vibration bands from polyglucose and other biological macromolecules superimposed on the broad continuum absorption features of the aqueous liquid. To minimize inter-experimental uncertainties, only cells that exhibited spectral features within one standard deviation of the mean (Fig. 2B) were selected for the oxygen-stress adaptive response experiments and the controls. We used the spectrally integrated absorption intensity of the polyglucose υC-OH band between ~1055 and ~1045 cm^{-1} to monitor polyglucose degradation. The intensity of the combination band δOH +υ_LHOH at ~2100 cm^{-1} tracks changes in water content because biomolecules typically show very little absorbance in the δOH +υ_LHOH region (31); the intensity of this band represents water concentration in biological samples (32). To

detect changes in the hydrogen-bonded structures in cellular water as a measure of transient chemical environment in living *D. vulgaris*, we first derived the FTIR time-difference spectra (relative to the initial state, t = 0) in the hydride-OH dominated stretch region between 1900 and 3800 cm^{-1} from the measured real-time FTIR spectra. In each time-difference spectrum, we minimize the water continuum absorbance; a positive absorption band reflects the formation of intermediates while a negative band the depletion of an initial state. To interpret changes observed in the FTIR time-difference spectra and to link them to the presence of ions and other small molecules, we used results from previous infrared simulation studies and infrared measurements on aqueous liquid and water clusters (15-19, 21-23). Because water molecules simultaneously can be hydrogen donors and acceptors, whether the water be liquid or small clusters (33, 34), spectral information from vibrational spectra of water clusters can be applied to understand dynamics in liquid or other condensed phases (34) such as water in the cellular environment.

Real-time FTIR spectromicroscopy of oxygen-stress adaptive response in live *D. vulgaris*. We monitored cells first under anaerobic conditions and then exposed to air. The measurements are shown in Figures 3 and 4, respectively, with comparisons shown in Figures 4C-E. The experiments proceeded as follows. We first made real-time FTIR measurements on a monolayer of *D. vulgaris* inside the oxygen-free humidified microscope stage chamber (hereafter *D. vulgaris*(+polyG;-air)) every five minutes for 240 minutes without interruption. Figure 3A shows the real-time FTIR spectra. An easy way to analyze and understand the time-difference spectra is to make a two-dimensional time-frequency contour plot of the difference spectra in the hydride-OH stretch region, as shown in Fig. 3B (negative values are shown in dark blue) with difference spectrum snapshots below. The plot shows, for t < ~50 minutes, positive bands at ~3190 cm^{-1}

and at ~3645 cm^{-1} and a shoulder feature at ~3745 cm^{-1}. These frequencies are in the υOH

regions of H-bonded structures of water molecules surrounded by hydrogen gas H$_2$ (i.e.

hydrogen hydrates) (14). This increasing positive behavior suggests a temporarily enhanced

hydrogen gas production event, which is consistent with the central metabolism of *D. vulgaris*

under anaerobic conditions (24, 35). This spectral information is taken as reference.

Using the same methodology, we then examined the survival of similar *D. vulgaris* (*D.*

vulgaris(+polyG;+air)) in atmospheric oxygen. We began by making FTIR measurements of *D.*

vulgaris in an anaerobic atmosphere for 30 minutes before introducing sterile air at t = 0. Unlike

the quiescent FTIR spectra from *D. vulgaris*(+polyG;-air) (Fig. 3A), these spectra show dramatic

variations over time (Fig. 4A). The two-dimensional time-frequency contour plot of the time-

difference spectra in the hydride-OH stretch region is shown in Fig. 4B with time-difference

spectrum snapshots below.

Spectrally integrated absorption intensities of water and polyglucose bands are shown in

Figures 4C and 4D. Under anaerobic conditions, the intensity of the combined water OH

bending and libration modes (blue circles in Fig. 4C) and the polyglucose C–OH vibration band

(blue circles in Fig. 4D) exhibit little change, but after air exposure they exhibit a multi-phasic

pattern. There is a reproducible "jump" in the water band intensity (green inverted triangles in

Fig. 4C) upon air exposure, which can result from a contribution due to periplasmic oxygen

reduction to water by cytochrome c_3 with existing intracellular H$_2$ (36, 37), since we observed H$_2$

was produced during anaerobic metabolism (see Fig. 3B). Then, from t > 0 to < ~50 minutes,

there is a substantial decrease in the polyglucose band intensity but little change in the water

band intensity. Polyglucose oxidation by *D. vulgaris*(+polyG;+air) may contribute to this

substantial polyglucose decline. We performed an independent carbohydrate analysis of similar

D. vulgaris exposed to humid air which showed a more than 30% decrease in carbohydrate in

cells in the first hour of air exposure. At t > ~50 minutes, the water band intensity increases

abruptly (Fig. 4C); the rate of polyglucose disappearance slows at later times (t > ~100 minutes)

(Fig. 4D). For an elucidation of the mechanism(s) underlying this behavior, it is crucial to

analyze the time-difference spectra in the hydride-OH region carefully.

   As seen in Figure 4B, between t > 0 and < ~50 minutes there are two large increasingly

positive absorption bands, and the band positions are in the region of the υOH of a water

molecule H-bonding with a carboxylic acid or carboxylate: the band between ~3500 and 3300

cm^{-1} corresponds to the υOH of a water molecule H-bonding loosely with the alcohol OH group

(19), and the band between ~3000 and 2600 cm^{-1} corresponds to the υOH of a water molecule

tightly H-bonded to a carboxyl (C=O) group (19). Polyglucose oxidation by desulfovibrios to

acetate (a two-carbon carboxylate) (9, 38) may contribute to these two large increasingly positive

bands. The significant increase with time in the peak intensity of acetate observed (labeled as

green circles in Fig. 4E) and the concurrent decrease in the polyglucose band intensity (inverted

green triangles in Fig. 4D) suggest that *D. vulgaris*(+polyG;+air) oxidizes polyglucose rapidly to

acetate, which it initially accumulates.

   The noticeable disappearance of these two acetate υOH bands at t > ~50 minutes (Fig. 4B)

implies disappearance of acetate (see also green circles in Fig. 4E), even though polyglucose

degradation continues for a time (green inverted triangles in Fig. 4C). Meanwhile, a new broad

υOH band begins to appear at frequencies between ~2750 and ~2550 cm^{-1} in the region of a

water molecule H-bonded with CO_2 (39) (see reference list in #39) to form carbonic acid (blue

triangles in Fig. 4E). The most likely explanation of this co-incidence at t > ~50 minutes

(compare the green circles for acetate and the blue triangles for CO_2 in Fig. 4E) is a conversion

of acetate to CO_2 (with increasing water content in cells; see inverted green triangles in Fig. 4C). This co-incidence suggests an onset of an adenosine triphosphate (ATP) generating pathway, possibly via C_1 intermediates (40). Other pathways would be the tricarboxcylic acid (TCA) cycle or the glyoxylate shunt, though they are less likely to occur since *D. vulgaris* lacks the genes for the production of key enzymes required in these cycles (24, 41).

Also appearing at t > ~50 minutes is an intense positive υOH band between ~3200 and ~3030 cm^{-1}, which is typical of a water molecule that forms a strong ionic H-bond with species such as the superoxide anion (16), hydroxyl radicals (15, 17, 18), and the hydroperoxyl radicals (22). This suggests that the formation of ROS exceeds their removal by the protective enzymes and other mechanisms in *D. vulgaris*(+polyG;+air) at this time (red squares in Fig. 4E).

At t = ~70 minutes a striking new υOH band begins to appear between ~3630 and ~3520 cm^{-1} in the spectral region of water molecules H-bonded to sulfate anions (23). Its notable persistence in intensity (pink hexagons in Fig. 4E) is consistent with previous observation that *D. vulgaris* can oxidize its accumulated elemental sulfur and other reduced sulfur compounds (42, 43). It has been suggested that the oxidation is by means of an adenosine triphosphate/adenyl sulfate (ATP/APS) pathway that couples the sulfate ion formation with oxygen reduction to water (42, 43). Consider that sulfate formation is an acidification reaction which produces protons (H^+), it is interesting that this acidification process coincides with the disappearance of ROS (compare the pink hexagons to the red squares in Fig. 4E) and the increase of water content (green inverted triangles in Fig. 4D).

There is increasing spectral complexity after t = ~70 minutes, as suggested by the pattern of the contours in Fig. 4B. The complexity includes progressive band broadening (~100 cm^{-1}) and a redshift (~250 cm^{-1}) in the existing υOH band of the water···ROS system (between ~3200 and

3030 cm^{-1}) as well as the water$\cdots$CO$_2$ system (at frequencies $< \sim$2650 cm^{-1}). This may arise partly from an increase in water molecules available to H-bond with either other anions or neutral species in *D. vulgaris*(+polyG;+air), or other more complicated factors that distort the spectral character (44, 45). For longer times (t $> \sim$150 minutes), the intensity of the υOH band of the water$\cdots$ROS declines (red squares in Fig. 4E), which suggests an improved ROS removal in *D. vulgaris*(+polyG;+air).

Confirmation. To confirm our results, we therefore used the same method and examined how the FTIR spectra in the hydride-OH dominated stretch region would differ in *D. vulgaris* that had not accumulated intracellular polyglucose granules (hereafter *D. vulgaris*(–polyG;+air)). Unlike the *D. vulgaris*(+polyG;+air), a positive broad υOH feature appeared immediately in the frequency range associated with the ionic H-bond with anionic ROS (15-18, 22) (Fig. 5). The feature broadened by several hundreds of cm^{-1} towards lower frequencies, and reflects an initial disordered ensemble of many different OH stretching vibration modes. The ROS formation continued to exceed their removal with air exposure time, as demonstrated by the monotonically increasing intensity and gradual redshifts of the vibration modes (centered at $\sim$3100 cm^{-1} initially to $\sim$3050 cm^{-1} at later times). The immediate positive feature detected at $\sim$3570 cm^{-1} (the red trace in Fig. 5) is within the spectral region of water molecules H-bonded to sulfate anions (23). This small positive value is consistent with our earlier observation that *D. vulgaris* in exponential phase accumulates little elemental sulfur. Little growth was detected when these *D. vulgaris* were returned to oxygen-free conditions.

Conclusions and implications. Our interpretation of the υOH bands in the FTIR time-difference spectra along with the time-course of the polyglucose υC-OH and the water (δOH +υ_LHOH) band intensities is summarized in Fig. 6. Considering the complexity of a living bacterial system,

the consistency of the spectral features and the agreement with the putative events of oxygen-stress adaptive response is striking. We have thus demonstrated both the efficacy of using the hydrogen bonding in water of living cells to profile intracellular chemical environment and their significant consequences for understanding functional metabolic controls in "obligate" anaerobic bacteria that can survive oxygen-stress transiently at the chemical level, by providing the first direct observations of molecular events measured in the same cells over time. Together, these FTIR experiments have revealed a remarkable sequence of well-orchestrated mechanisms that some *D. vulgaris* use to temporarily survive oxygen exposure. When extending this approach to other adaptive-response cellular systems, the experimental design and interpretation of the data should be straightforward in cases where transient chemistry is dominated by ions or other small chemical species. Even in more complex cases, we anticipate that the interpretation of infrared spectroscopic data in terms of the hydrogen-bonded structure of cellular water will open the door to investigations of chemical and molecular structural changes in living bacteria and other cellular systems over the course of their stress-adaptive response.

Materials and Methods

Bacterial strains and culture. *Desulfovibrio vulgaris* Hildenborough (ATCC 29579) was obtained from the American Type Culture Collection (Manassas, VA). All *D. vulgaris* used in this study were cells of second passage grown on a defined lactate sulfate medium (LS4D medium) soft agar plate (1.0% wt/vol). The LS4D medium was based on Postgate's medium C. To prepare stationary-phase *D. vulgaris* population, we grew *D. vulgaris* (at high cell density) anaerobically on soft LS4D agar until the growth of some bacterial colonies reached confluence. Most cells from the confluent colonies exhibited infrared spectral characteristics typical of polyglucose-containing *D. vulgaris* (red trace in Fig. 1A). To prepare exponential-phase *D.*

vulgaris population, we grew *D. vulgaris* (at low cell density) anaerobically on LS4D agar until the growth of bacterial colonies first became visible. Cells from these microcolonies mostly did not exhibit infrared spectral characteristics typical of polyglucose-containing *D. vulgaris* (blue trace in Fig. 1A).

Preparation of *D. vulgaris* monolayers. To ensure that each *D. vulgaris* cell in the FTIR experiment was in contact with atmospheric oxygen, we prepared micron-thick layers of *D. vulgaris*. We transferred *D. vulgaris* cells onto a LS4D-treated gold-coated glass wafer. An additional mist of liquid LS4D was applied to the replica-printed wafer, which was then incubated for an additional 24 hours to facilitate migration of mobile cells to form monolayers on the LS4D-treated gold-coated glass wafer under suitable conditions. To assess the morphological quality of the monolayers, the wafer was placed in a custom microscope stage chamber (filled with nitrogen gas), and was observed by oblique illumination microscopy. Prior to the FTIR experiment, any excess (moving) LS4D medium was removed by wicking.

High-resolution FTIR spectromicroscopy. We built a high-humidity microscope stage chamber (Fig. 2A) that allows one to maintain a constant micron-thick layer of live *D. vulgaris*, overcoming the water interference during high-resolution FTIR spectromicroscopy measurements. All measurements were performed with a Nicolet Magna 760 FTIR bench and a Nicolet Nic-Plan IR microscope (Thermo Scientific, MA, USA) equipped with a microscope stage chamber at the infrared beamline of the Advanced Light Source (Lawrence Berkeley National Laboratory, CA, USA; http://infrared.als.lbl.gov/). Each spectrum represents an average of 64 scans over a wavenumber range of 4000 to 650 cm^{-1} at a spectral resolution of 4 cm^{-1} with an absorption peak position accuracy of 1/100 cm^{-1}. As the beam current of the synchrotron decreases with time between electron refills (nine hours), the beam intensity decreases

proportionally. Appropriate baseline removal took this into account. All data processing was performed using Thermo Electron's Omnic 7.2 (http://www.thermo.com/) and Origin 6.0 (http://www.originlab.com/). Time-difference spectra are calculated (using Thermo Electron's Omnic 7.2 software (http://www.thermo.com/)) from experimental spectra after subtraction of culture medium/liquid water absorbance (46). The time-difference spectra calculation was performed using the water factor approach (47) to minimize absorbance of the water continuum. Analysis of time difference spectra is described in the main text.

Carbohydrate analysis. Cell pellets were collected from air exposure experiments and were re-suspended in 1 ml of 0.7% NaCl (wt/vol). Protein concentrations were determined with the Lowry assay using bovine serum albumin (Pierce Biochemicals) as the standard (48). Hexose sugars were measured using the colorimetric cysteine-sulfuric acid method (49) with glucose as the standard.

Live/dead fluorescence microscopy for distinguishing live and dead bacteria. The LIVE/DEAD BacLight bacterial viability kit (Molecular Probes, Oregon, USA) in combination with a fluorescence microscope (Zeiss Axioskop, Germany) was used. Here, cells were exposed to air for t = 0, 30, 240, and 480 minutes; and the level of internalized red fluorescing propidium relative to green fluorescing SYTO9 allowed for differentiation between *D. vulgaris* with intact cytoplasmic membranes (bright green) and *D. vulgaris* with damaged cytoplasmic membranes (red/yellow) (50).

Electron microscopy. For conventional preparations, *D. vulgaris* were fixed, embedded, thin sectioned and post-stained by the periodic acid thiosemicarbazide-osmium (PATO) exactly as previously described (51). Preparation and imaging were conducted at the Robert D. Ogg Electron Microscope Lab at the University of California, Berkeley, CA (http://em-

lab.berkeley.edu/EML/index.php). Cryo-EM samples were made by placing 5-μl aliquots of the D. vulgaris suspension onto lacey carbon grids (Ted Pella 01881) that were pre-treated by glowdischarge, then blotting and plunging into liquid ethane. Images were recorded on a JEOL-3100 electron microscope operated at 300 kV by a Gatan 795 CCD camera at a magnification of 30,000x. Samples to be used for EDX analysis were freeze-dried in the microscope's airlock and then examined in an FEI CM-200 microscope equipped with a Link EDX detector. Re-growth experiment. The re-growth experiments were to obtain growth curves of control (anaerobic) versus air-exposed cells when returned to oxygen-free conditions. Stressed and control cells grown from the oxygen stress experiment were removed from the culture bottles after 24 hours of either N2 or air purge. 10 μL of culture was added to 100 μL of LS4D medium in wells of an empty microplate. Eight replicate wells were used for each culture. Cells were incubated in the Omnilog (Biolog, Hayward, CA) anaerobically at 30oC for 100 hours. Increase in cell density was quantified by recording increased opacity caused by the accumulation of FeS precipitates. The Omnilog uses a scanning technology, which is analogous to a turbidity measurement, to record the increase in density in Omnilog (OL) units.

References

1. Fay, P. (1992) Oxygen relations of nitrogen-fixation in Cyanobacteria. *Microbiol Rev* 56(2):340-373.

2. Bradshaw, D.J., Marsh, P.D., Watson, G.K., & Allison, C. (1998) Role of *Fusobacterium nucleatum* and coaggregation in anaerobe survival in planktonic and biofilm oral microbial communities during aeration. *Infect Immun* 66(10):4729-4732.

3. Cypionka, H. (2000) Oxygen respiration by *Desulfovibrio* species. *Annu Rev Microbiol* 54:827-848.

4. Baughn, A.D. & Malamy, M.H. (2004) Molecular Basis for Aerotolerance of the Obligately Anaerobic *Bacteroides* Spp. *Strict and Facultative Anaerobes: Medical and Environmental Aspects*, eds Nakano, M.M. & Zuber, P. (CRC Press, New York), pp 161-169.

5. Dolla, A., Fournier, M., & Dermoun, Z. (2006) Oxygen defense in sulfate-reducing bacteria. *J Biotechnol* 126(1):87-100.

6. Brioukhanov, A.L. & Netrusov, A.I. (2007) Aerotolerance of strictly anaerobic microorganisms and factors of defense against oxidative stress: A review. *Appl Biochem Micro+* 43(6):567-582.

7. Muyzer, G. & Stams, A.J.M. (2008) The ecology and biotechnology of sulphate-reducing bacteria. *Nat Rev Microbiol* 6(6):441-454.

8. Fuseler, K. & Cypionka, H. (1995) Elemental Sulfur as an Intermediate of Sulfide Oxidation with Oxygen by *Desulfobulbus Propionicus*. *Arch Microbiol* 164(2):104-109.

9.   Van Niel, E.W.J.*, et al.* (1996) The role of polyglucose in oxygen-dependent respiration by a new strain of *Desulfovibrio salexigens*. *Fems Microbiol Ecol* 21(4):243-253.

10.   Fareleira, P.*, et al.* (2003) Response of a strict anaerobe to oxygen: survival strategies in *Desulfovibrio gigas*. *Microbiology* 149(Pt 6):1513-1522.

11.   Holman, H.-Y.N. & Martin, M.C. (2006) Synchrotron radiation infrared spectromicroscopy: a non-invasive molecular probe for biogeochemical processes. *Advances in Agronomy*, ed Sparks, D. (Elsevier, New York), Vol 90, pp 79-127.

12.   Woutersen, S. & Bakker, H.J. (1999) Resonant intermolecular transfer of vibrational energy in liquid water. *Nature* 402(6761):507-509.

13.   Cowan, M.L.*, et al.* (2005) Ultrafast memory loss and energy redistribution in the hydrogen bond network of liquid H_2O. *Nature* 434(7030):199-202.

14.   Okumura, M., Yeh, L.I., Myers, J.D., & Lee, Y.T. (1990) Infrared-spectra of the solvated hydronium ion - vibrational predissociation spectroscopy of mass-selected $H_3O^+.(H_2O)_n.(H_2)_m$. *J Phys Chem-Us* 94(9):3416-3427.

15.   Nelander, B. (1997) The peroxy radical as hydrogen bond donor and hydrogen bond acceptor: A matrix isolation study. *J Phys Chem A* 101(48):9092-9096.

16.   Weber, J.M.*, et al.* (2000) Isolating the spectroscopic signature of a hydration shell with the use of clusters: Superoxide tetrahydrate. *Science* 287(5462):2461-2463.

17.   Chaudhuri, C.*, et al.* (2001) Infrared spectra and isomeric structures of hydroxide ion-water clusters $OH^- (H_2O)_{(1-5)}$: a comparison with $H_3O^+ (H_2O)_{(1-5)}$. *Mol Phys* 99(14):1161-1173.

18.   Robertson, W.H.*, et al.* (2003) Spectroscopic determination of the OH^- solvation shell in the $OH^-.(H_2O)_{(n)}$ clusters. *Science* 299(5611):1367-1372.

19.   Max, J.J. & Chapados, C. (2004) Infrared spectroscopy of aqueous carboxylic acids:

       Comparison between different acids and their salts. *J Phys Chem A* 108(16):3324-3337.

20.   Shin, J.W.*, et al.* (2004) Infrared signature of structures associated with the $H^+(H_2O)_{(n)}$

       (n=6 to 27) clusters. *Science* 304(5674):1137-1140.

21.   Headrick, J.M.*, et al.* (2005) Spectral signatures of hydrated proton vibrations in water

       clusters. *Science* 308(5729):1765-1769.

22.   Iyengar, S.S. (2005) Dynamical effects on vibrational and electronic spectra of

       hydroperoxyl radical water clusters. *J Chem Phys* 123(8):084310-084311-084310.

23.   Bush, M.F., Saykally, R.J., & Williams, E.R. (2007) Evidence for water rings in the

       hexahydrated sulfate dianion from IR spectroscopy. *J Am Chem Soc* 129(8):2220-2223.

24.   Heidelberg, J.F.*, et al.* (2004) The genome sequence of the anaerobic, sulfate-reducing

       bacterium *Desulfovibrio vulgaris* Hildenborough. *Nat Biotechnol* 22(5):554-559.

25.   Baumgartner, L.K.*, et al.* (2006) Sulfate reducing bacteria in microbial mats: Changing

       paradigms, new discoveries. *Sediment Geol* 185(3-4):131-145.

26.   Chapple, I.L.C. (1996) Role of free radicals and antioxidants in the pathogenesis of the

       inflammatory periodontal diseases. *J Clin Pathol-Cl Mol* 49(5):M247-M255.

27.   Duffy, M.*, et al.* (2002) Sulfate-reducing bacteria colonize pouches formed for ulcerative

       colitis but not for familial adenomatous polyposis. *Dis Colon Rectum* 45(3):384-388.

28.   Risatti, J.B., Capman, W.C., & Stahl, D.A. (1994) Community Structure of a Microbial

       Mat - the Phylogenetic Dimension. *P Natl Acad Sci USA* 91(21):10173-10177.

29.   Minz, D.*, et al.* (1999) Diversity of sulfate-reducing bacteria in oxic and anoxic regions

       of a microbial mat characterized by comparative analysis of dissimilatory sulfite

       reductase genes. *Appl Environ Microb* 65(10):4666-4671.

30.   Stams, F.J.M., Veenhuis, M., Weenk, G.H., & Hansen, T.A. (1983) Occurrence of
      Polyglucose as a Storage Polymer in Desulfovibrio Species and Desulfobulbus-
      Propionicus. *Archives of Microbiology* 136(1):54-59.

31.   Naumann, D. (2000) Infrared Spectroscopy in Microbiology. *Encycloedia of Analytical
      Chemistry*, ed Meyers, R.A. (John Wiley & Sons Ltd, Chichester), pp 102-131.

32.   Potts, R.O., Guzek, D.B., Harris, R.R., & Mckie, J.E. (1985) A non-invasive, in vivo
      technique to quantitatively measure water concentration of the stratum-corneum using
      attenuated total-reflectance infrared-spectroscopy. *Arch Dermatol Res* 277(6):489-495.

33.   Vernon, M.F.*, et al.* (1982) Infrared vibrational predissociation spectroscopy of water
      clusters by the crossed laser-molecular beam technique. *J Chem Phys* 77(1):47-57.

34.   Castleman, A.W. & Keesee, R.G. (1986) Clusters - Bridging the gas and condensed
      phases. *Accounts Chem Res* 19(12):413-419.

35.   Tsuji, K. & Yagi, T. (1980) Significance of hydrogen burst from growing cultures of
      Desulfovibrio vulgaris, Miyazaki, and the role of hydrogenase and cytochrome c_3 in
      energy-production system. *Arch Microbiol* 125(1-2):35-42.

36.   Baumgarten, A., Redenius, I., Kranczoch, J., & Cypionka, H. (2001) Periplasmic oxygen
      reduction by *Desulfovibrio* species. *Arch Microbiol* 176(4):306-309.

37.   Fitz, R.M. & Cypionka, H. (1991) Generation of a proton gradient in *Desulfovibrio
      vulgaris*. *Arch Microbiol* 155(5):444-448.

38.   Santos, H.*, et al.* (1993) Aerobic metabolism of carbon reserves by the obligate anaerobe
      Desulfovibrio gigas. *Biochem Bioph Res Co* 195(2):551-557.

39.   Brucato, J.R., Palumbo, M.E., & Strazzulla, G. (1997) Carbonic acid by ion implantation
      in water/carbon dioxide ice mixtures. *Icarus* 125(1):135-144.

40.   Schauder, R*., et al.* (1986) Acetate oxidation to CO_2 in anaerobic bacteria via a novel pathway not involving reactions of the citric-acid cycle. *Arch Microbiol* 145(2):162-172.

41.   Tang, Y*., et al.* (2007) Pathway confirmation and flux analysis of central metabolic pathways in *Desulfovibrio vulgaris* hildenborough using gas chromatography-mass spectrometry and Fourier transform-ion cyclotron resonance mass spectrometry. *J Bacteriol* 189(3):940-949.

42.   Kramer, M. & Cypionka, H. (1989) Sulfate formation via ATP sulfurylase in thiosulfate-disproportionating and sulfite-disproportionating bacteria. *Arch Microbiol* 151(3):232-237.

43.   Fuseler, K., Krekeler, D., Sydow, U., & Cypionka, H. (1996) A common pathway of sulfide oxidation by sulfate-reducing bacteria. *Fems Microbiol Lett* 144(2-3):129-134.

44.   Lawrence, C.P. & Skinner, J.L. (2003) Vibrational spectroscopy of HOD in liquid D_2O. III. Spectral diffusion, and hydrogen-bonding and rotational dynamics. *J Chem Phys* 118(1):264-272.

45.   Yamashita, T. & Takatsuka, K. (2007) Hydrogen-bond assisted enormous broadening of infrared spectra of phenol-water cationic cluster: An *ab initio* mixed quantum-classical study. *J Chem Phys* 126(7):-.

46.   Mantele, W. (1993) Reaction-induced infrared difference spectroscopy for the study of protein function and reaction-mechanisms. *Trends Biochem Sci* 18(6):197-202.

47.   Max, J.J. & Chapados, C. (2002) Infrared spectroscopy of aqueous carboxylic acids: Malic acid. *J Phys Chem A* 106(27):6452-6461.

48.   Lowry, O.H., Rosebrough, N.J., Farr, A.L., & Randall, R.J. (1951) Protein measurement with the folin phenol reagent. *J Biol Chem* 193(1):265-275.

49.   Chaplin, M.F. (1986) Monosaccharides. *Carbohydrate analysis*, eds Chaplin, M.F. &

        Kennedy, J.F. (IRL Press, Oxford), pp 1-4.

50.   Leuko, S., Legat, A., Fendrihan, S., & Stan-Lotter, H. (2004) Evaluation of the

        LIVE/DEAD BacLight kit for detection of extremophilic archaea and visualization of

        microorganisms in environmental hypersaline samples. *Appl Environ Microb*

        70(11):6884-6886.

51.   Kropinski, A.M., Ghiorse, W.C., & Greenberg, E.P. (1988) The intracellular polyglucose

        storage granules of *Spirochaeta aurantia*. *Arch Microbiol* 150(3):289-295.

Figure legends

Fig. 1. Microscopic and spectroscopic analyses of *Desulfovibrio vulgaris*. (A) Left, typical infrared absorption spectra of stationary-phase (red) and exponential-phase (blue) *D. vulgaris*; right, transmission electron microscopy (TEM) images of thin sections post-stained by the periodic acid thiosemicarbazide-osmium (PATO) method (51) show intracellular polyglucose granules (arrows) in stationary-phase but not exponential-phase *D. vulgaris*. (B) Left, cryo-electron microscopy (Cryo-EM) image of a stationary-phase cell containing a large, dense ball; right, energy dispersive x-ray analysis of freeze-dried cells with (blue) and without (red) such structures. Spectra from areas such as marked by the blue circle in the left image show that the particle contains mainly sulfur. (C) Re-growth of *D. vulgaris* after exposure to air. Note the ~20-hour lag-time (compared to controls). Different colors represent different viability experiments. (D, E) Cryo-EM (left) and TEM/PATO (right) images of *D. vulgaris* after exposure to air for hours show changes in cell membranes, variation in periplasmic space, mottled appearance of

cell contents and decreased number of polyglucose granules compared to the unexposed cell in

Figs. 1A and 1B. The frequency of cells showing such alterations compared to those with

substantially more damage suggests that these cells were still alive. Scale bar, 0.2 µm.

Fig. 2. FTIR measurement setup. (A) Schematic description of the experimental measurement

setup**.** An all-reflective optics infrared microscope focuses the interferometer-modulated

synchrotron infrared micro-beam through a 15–µm aperture onto a monolayer (see methods) of

live *D. vulgaris*. The reflected signals are collected and sent to the detector. The optical density

of this thin film is typically ~0.05 at the band dominated by the combined water-bending

vibration and libration at ~2100 cm^{-1}. This is an equivalent to a water-film of ~1.5-micron thick.

This experimental system enables FTIR measurements with a temporal resolution of every

minute for up to four hours; a different experimental arrangement would be needed to investigate

changes on a finer temporal scale or a longer duration. (B) Spectral variations in polyglucose-

accumulated stationary-phase *D. vulgaris* in anaerobic atmosphere. The spectrum shows the

polyglucose C–OH vibration (υC–OH) band between 1055 and 1045 cm^{-1}. Within the hydride-

OH dominated stretch region between 1900 and 3800 cm^{-1} are a broad OH stretching (υOH)

band between 2900 and 3700 cm^{-1}, the combined water OH bending and libration modes (δOH

$+υ_L$HOH) at ~2100 cm^{-1}. Absorption bands between 1800 and 900 cm^{-1} are dominated by

vibration motion of biomolecules of *D. vulgaris*. Averaged spectrum (black line) ± 1.0 standard

deviation (gray line); n = 50.

Fig. 3. FTIR analyses of *D. vulgaris* in anaerobic atmosphere. (A) Real-time FTIR spectra of

polyglucose-accumulated stationary-phase *D. vulgaris* in an anaerobic environment. Sequential

spectra are offset vertically for clarity. Since all spectra are derived using air as a reference, the

negative spectral feature at ~2348 cm^{-1} (associated with lack of atmospheric CO_2) is a marker for

an air-free condition throughout this investigation. (B) FTIR time-difference spectra in the hydride-OH dominated stretch region. Top, a 2-dimensional frequency-time contour plot (the time-difference intensities are normalized to the maximum); bottom, snapshots for selected different time points. Positive bands (labeled as υOH(water$\cdots$H$_2$)) arise from υOH of water molecules forming H-bonding with H$_2$ (~3190; ~3640, and ~3745 cm^{-1}).

Fig. 4. FTIR analyses of *D. vulgaris* during oxygen-stress adaptive response. (A) Typical real-time FTIR spectra of polyglucose-accumulated stationary-phase *D. vulgaris* transition from an anaerobic to aerobic environment. Sequential spectra are offset upward for clarity. Since all spectra are derived using air as a reference, the abrupt change in the spectral feature at ~ 2348 cm^{-1} associated with the presence of atmospheric CO$_2$. (B) Corresponding FTIR time-difference spectra in the hydride-OH dominated stretch region. Top, a 2-dimensional frequency-time contour plot (the time-difference intensities are normalized to the maximum); bottom, snapshots for selected different time points. Positive values arise from υOH of water molecules forming H-bonding with acetate (~3440; ~2930 cm^{-1}) (labeled as υOH(water$\cdots$acetate)), reactive oxygen species ROS (~3090 cm^{-1}) (labeled as υOH(water$\cdots$ROS)), sulfate (~3565 cm^{-1}) (labeled as υOH(water$\cdots$sulfate)), and carbonic acid (~2450 cm^{-1}) (labeled as υOH(water$\cdots$CO$_2$)). The positive absorption feature at ~2360 cm^{-1} is from CO$_2$ in air. (C, D). Typical time course of infrared intensity (normalized by the maximum value) of water and polyglucose content. Bar = ±10% error. (E) Transient chemistry as seen by the time-course of difference absorbance normalized by the maximum value for each species. Bar = ±10% error.

Fig. 5. Typical FTIR difference spectra show reactive oxygen species (ROS) build-up in polyglucose-deficient exponential-phase *D. vulgaris*. Top, a 2-dimensional frequency-time contour plot (the time-difference intensities are normalized to the maximum); bottom, snapshots

for selected different time points. The peak centered at ~3100 cm^{-1} and other local maxima centered at ~2904 cm^{-1} and ~2810 cm^{-1} are at frequencies typical of the υOH of water molecules H-bonding with hydroxyl and hydroperoxyl radicals (labeled as υOH(water$\cdots$ROS)). The feature at ~3570 cm^{-1} is at a frequency typical of the υOH of water molecules H-bonded to sulfate anions. Yellow dots mark the red-shift of ~75 cm^{-1} of υ_{OH} of hydroxyl radical band peak. The positive absorption feature at ~2360 cm^{-1} is from CO_2 in air.

Fig. 6. A summary of the evolving cellular chemical environment and possible survival mechanisms inside the same living *D. vulgaris* during its transient oxygen-stress and adaptive response, as revealed by the real-time high-resolution FTIR measurements and analyses. Polyglucose is labeled as PolyG.
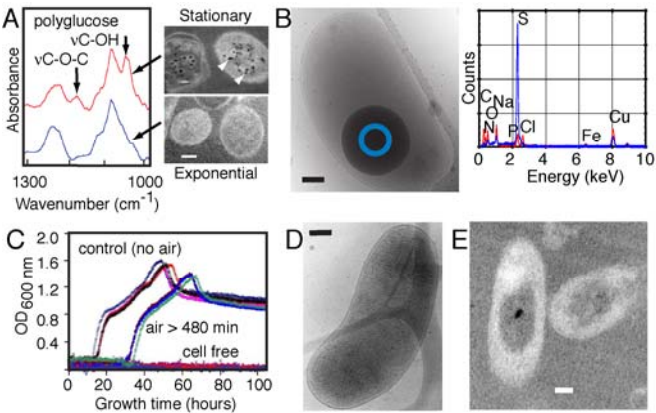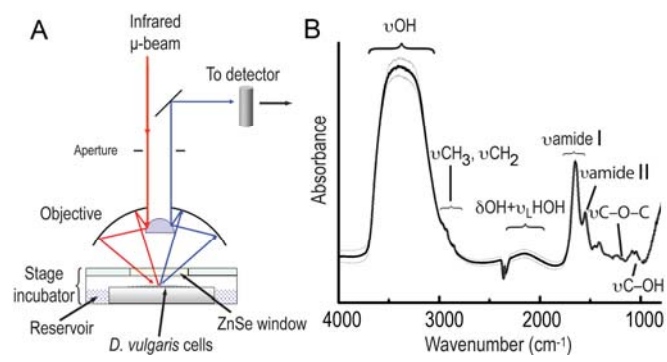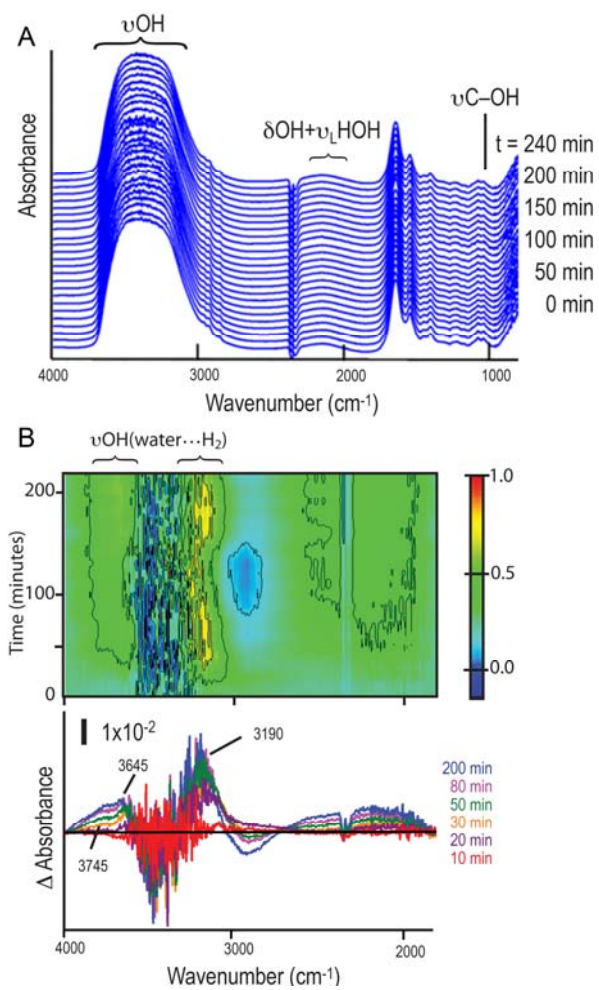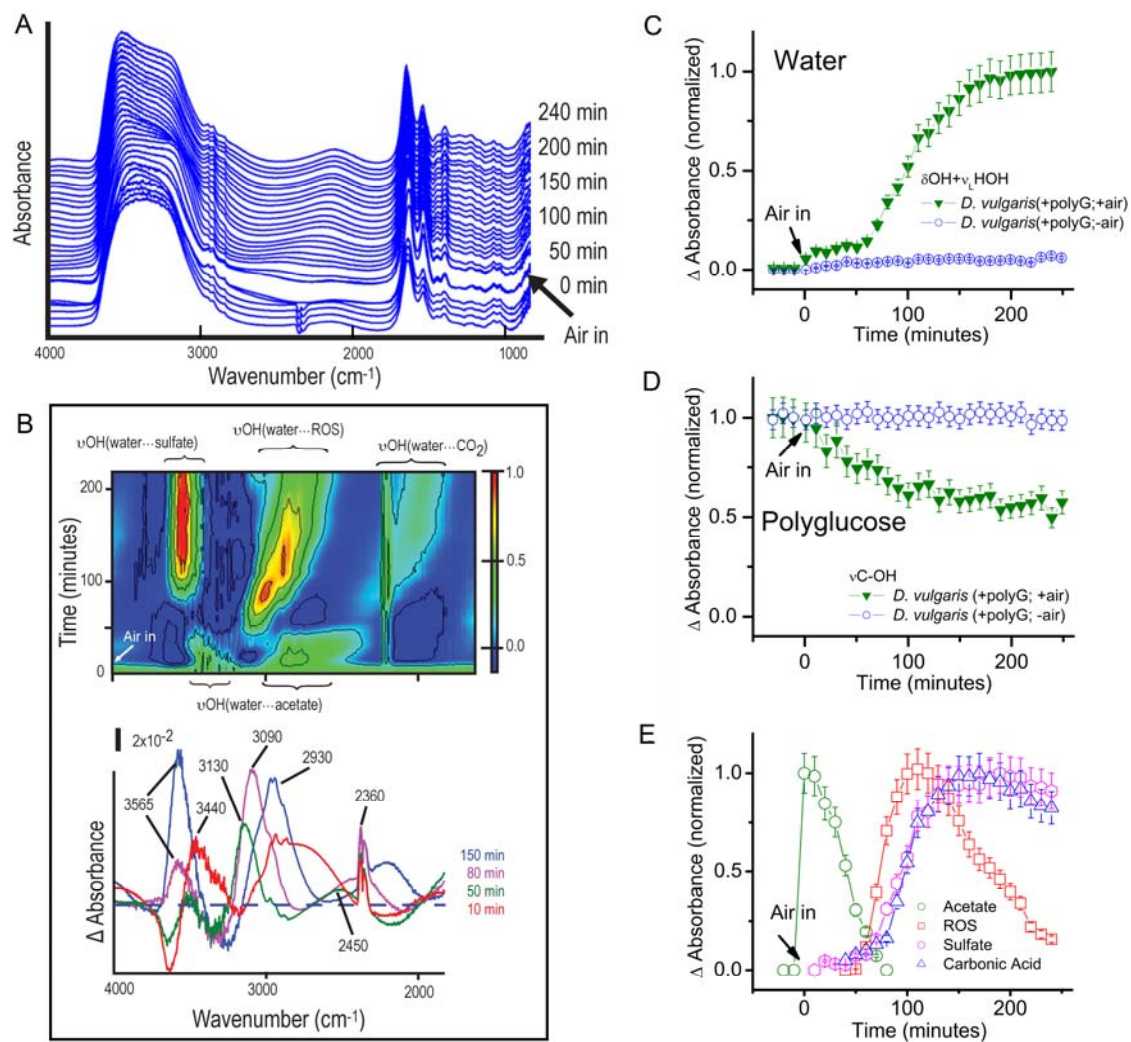
Figure 1

Figure 2

Figure 3

Figure 4

Figure 5

Figure 6

Anaerobic | **Aerobic**

Air in

Fermentation; H₂ production

Rapid polyG oxidation; rapid acetate production/ accumulation; little H₂O production (except for the initial burst)

Moderate polyG oxidation; acetate disappearance; rapid H₂O production+ CO₂ production (likely through the oxidative acetyl CoA pathway) rapid ROS accumulation

Rapid sulfate production (likely through the ATP/APS pathway with water production)

Little polyglucose oxidation; rapid H₂O production; moderate CO₂ production, rapid ROS consumption

H₂O production; ROS consumption

Time (minutes)

0   50   100   150   200